Cement and Concrete Composites 74 (2016) 164–173

Contents lists available at ScienceDirect

Cement and Concrete Composites

journal homepage: www.elsevier.com/locate/cemconcomp

The influence of cellulose nanocrystals on the microstructure of cement paste

Yizheng Cao [a], Nannan Tian [b], David Bahr [b], Pablo D. Zavattieri [c], Jeffrey Youngblood [b], Robert J. Moon [d], Jason Weiss [e, *]

[a] SSCI, Albany Molecular Research Inc., West Lafayette, IN 47906, USA
[b] School of Materials Engineering, Purdue University, West Lafayette, IN 47907, USA
[c] Lyles School of Civil Engineering, Purdue University, West Lafayette, IN 47907, USA
[d] Forest Products Laboratory, US Forest Service, Madison, WI 53726, USA
[e] School of Civil and Construction Engineering, Oregon State University, OR 97331, USA

ARTICLE INFO

Article history:
Received 16 January 2016
Received in revised form
22 September 2016
Accepted 26 September 2016
Available online 28 September 2016

Keywords:
Cellulose nanocrystal
Cement
Agglomeration
Ultrasonication
Flexural strength
Nanoindentation

ABSTRACT

This paper reports the influence of raw and sonicated cellulose nanocrystals (CNCs) on the microstructure of cement paste. A novel centrifugation method is designed to measure the concentrations of the adsorbed CNCs (aCNCs) on the cement surface, and the free CNCs (fCNCs) which are mobile in water. It is found that, the majority of the CNCs (>94%) are aCNCs. More importantly, sonication does not significantly reduce the amount of aCNCs (reduction of less than 2%). We surmise that, after sonication, the aCNCs are primarily dispersed over the cement surface, instead of becoming fCNCs via sonication. Isothermal calorimetry and energy-dispersive X-ray spectroscopy (EDX) results support this theory. The water desorption tests show that the total porosities of cement pastes with raw and sonicated CNCs are 14.8% and 14.4%, which showed a reduction from 16% for the plain cement paste. The porosity reduction is a result of an increase in the degree of hydration. The advantage of sonicated CNCs is they are dispersed, avoiding therefore agglomerates that can lead to pores, voids, and air entrapment. The nanoindentation results show that the reduced indentation modulus on the interfacial regions between cement particles and the low density CSH is increased when CNCs are used.

1. Introduction

Cellulose nanocrystal (CNC) is the crystalline part of the cellulose materials, which can be extracted from trees and a variety of plants [1]. As a reinforcement material, CNC has a few extraordinary advantages, including biodegradability, high abundance, low cost, and excellent mechanical properties [1]. Recently, CNCs have been found to improve the flexural strength of cement composites due to an increase in the degree of hydration (DOH) [2] which is possibly aided by a mechanism referred to as short circuit diffusion (SCD). The basic prerequisite for SCD is the adsorption of CNCs on the surface of cement particles, acting as the pathway to preferentially transport water from pores to unhydrated cement cores. Such capability can be attributed to the high hydrophilicity and hygroscopicity of the CNCs [3]. A competing mechanism has also been identified for CNC concentrations larger than 0.2 vol % where agglomerates induce stress concentrators limiting the strength of the cement pastes [2]. This issue was subsequently addressed by Cao et al. [4] with ultrasonication (or sonication) to disperse the CNCs in the aqueous suspension before mixing with cement.

The concentration of the CNCs adsorbed on the cement particles is an important factor as it directly influences the SCD. For simplicity the CNCs in the fresh cement paste are categorized as two types: the “free” CNCs in the water and the “adsorbed” CNCs on cement surface (abbreviated as fCNCs and aCNCs, respectively) as illustrated in Fig. 1. While both types of CNCs are in solution, the main difference is that the aCNCs are hard to move, as they adhere to the cement particles and the fCNCs can freely move in the aqueous suspension. The classification and quantification of these two types of CNCs are important for four reasons: we hypothesize that (1) the SCD is primarily governed by the amount of aCNCs; and (2) the strength of the cement is largely limited by the CNC agglomeration; we also lack sufficient information about (3) the

* Corresponding author. School of Civil and Construction Engineering, Oregon State University, OR 97331, USA.
E-mail address: jason.weiss@oregonstate.edu (J. Weiss).

http://dx.doi.org/10.1016/j.cemconcomp.2016.09.008
0958-9465/

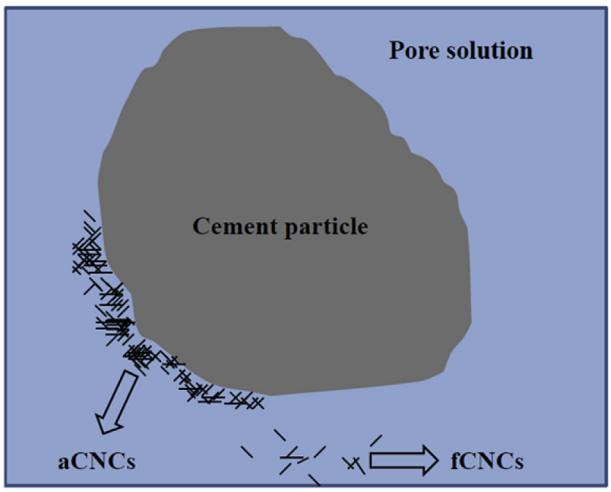

Fig. 1. The schematic of the two different types of CNCs in the fresh cement paste.

role the fCNCs on the cement properties; (4) the mobility of CNCs in the cement paste. We present a novel experimental approach to measure the concentrations aCNCs and fCNCs and their effect on SCD.

This paper focuses on the characterization of the cement pastes with raw and sonicated CNCs at the micro-level and studies how the dispersion of CNCs influences the microstructures of cement paste. A novel centrifugation experiment is designed to study the influence of sonication on the concentrations of fCNCs and aCNCs in the fresh cement paste. In addition, isothermal calorimetry is performed to provide the information on cement hydration with sonicated CNCs. For the hardened cement pastes (age of 28 days), nanoindentation is used to study how CNCs influence the elastic modulus and hardness of the three phases: unhydrated cement, interfacial region, and the low density CSH. In addition, SEM and EDX are employed to characterize the distribution of CNCs in the cement paste. Finally the water desorption test is used on the hardened cement pastes to study pore size distribution and how CNCs reduce the pores.

2. Materials and experimental testing

2.1. Materials

A Type V cement was used in this investigation due to its compositional purity (i.e., low aluminates and ferrite phases), the Bogue compositions and Blaine fineness of which are shown in Table 1.

The CNC materials used in this work were manufactured and provided by the USDA Forest Service-Forest Products Laboratory, Madison, WI, (FPL) [5]. The as-received CNC materials were in a form of freeze dried powders, 0.96 wt % sulfur on CNC. The CNCs were extracted using sulfuric acid hydrolysis of Eucalyptus dry-lap cellulose fibers, resulting in a 0.81 wt % CNC surface-grafted sulfate content.

Table 1
Bogue compositions of Type V cement.

C_3S (%)	63.8
C_2S (%)	13
C_3A (%)	0
$C_4AF + C_2F$ (%)	12.6
Blaine fineness, m^2/kg	316

2.2. Cement paste preparation

For cement past preparation, cement is added to the mixing container, then CNCs are added to the cement powder, and the final step is to add water to keep the water to cement ratio (w/c) at 0.35. The mixing procedures are described in the previous work [2] and the mixtures proportions are listed in Table 2.

Cement pastes with raw and sonicated CNCs are studied in this work. 30 min of sonication was performed to disperse the CNCs in the aqueous suspension, employing an ice water bath to minimize the possible desulfation [6,7]. This sonication technique and the experimental details can be found in the previous paper [4].

2.3. Centrifugation

A centrifugation method is established to quantify the concentrations of the aCNC and fCNC. At the age of 15 min (from the time of mixing), approximately 250 g fresh cement pastes are transferred into a Sorvall RC-3C Plus high capacity centrifuge. The centrifugation was performed at 5000 rpm for 20 min and the liquid on top of the cement was collected. The collected liquid was then filtered three times with filter paper to remove the cement particles. Previous control tests on the CNC aqueous suspensions showed that most of the CNCs (>99.5%) passed through the filter paper, and therefore the loss of CNCs due to filtration was not accounted for. The filtered liquid was then weighed and dried in an oven at 50 °C for 48 h. For the plain cement paste, the final products after oven-drying are the salts and alkalis in the pore solutions [8], while for the cement paste with CNCs, the solids also contain the fCNCs. By comparing the solids concentrations obtained from the two different cement pastes, the concentrations for the fCNCs as well as the aCNCs can be calculated.

2.4. Isothermal calorimetry

Isothermal calorimetry tests were performed to study how the sonication influences the hydration process of the cement pastes. A TAM Air isothermal calorimeter was used with a temperature of 23 ± 0.1 °C [9]. After the cement paste mixing, approximately 30 g of the sample was immediately transferred to a glass ampoule (22 mm in diameter and 55 mm in height), which was then sealed and placed into the calorimeter for measurement. Before the data collection started, the isothermal condition was held for 45 min to reach equilibration and the subsequent steady heat measurement was performed for approximately 200 h.

2.5. Nanoindentation

One link between the CNC distribution in the cement paste and the mechanical performance at the macro-level, e.g., the flexural strength, is the CNCs influence on the microstructural mechanical properties. To investigate the local variations of the material behavior within cement microstructures nanoindentation has been used in the areas of interfacial transition zone in concrete [10] to study the micro-mechanisms of creep in CSH phases [11], and conduct statistical analysis of the nano-mechanical properties governing the ultra-high performance concrete microstructure [12]. As CNCs have completely different materials properties from cement, they may alter the microstructural properties of cement paste, e.g. elastic modulus and hardness, and these changes may vary significantly with higher concentration of CNCs. For this reason, the microstructural properties may be indicative of the CNCs distribution in the cement pastes. Since CNCs are prone to adsorb on cement surface, a high concentration is expected to be found in the high density CSH region for a hardened cement paste.

Table 2
Experimental matrix for cement pastes with CNCs.

Mixture ID	wt (g)			vol (cm^3)			CNC/cement
	Cement	CNC	Water	Cement	CNC	Water	vol %
1 (ref)	500	0	175	160.3	0	175	0.00%
2	500	0.103	175	160.3	0.064	175	0.04%
3	500	0.256	175	160.3	0.16	175	0.10%
4	500	0.513	175	160.3	0.321	175	0.20%
5	500	1.282	175	160.3	0.801	175	0.50%
6	500	2.564	175	160.3	1.603	175	1.00%
7	500	3.846	175	160.3	2.404	175	1.50%

In this work, nanoindentation was performed at three different phases in the hardened cement pastes: the unhydrated cement particle, high density CSH and low density CSH to study how the mechanical properties were influenced by CNCs. The mechanical properties obtained from nanoindentation were the reduced indentation modulus E_r and hardness H.

Three different cement pastes samples were prepared for the nanoindentation: plain (reference), one with 1.5 vol % raw CNCs and one with 1.5 vol % sonicated CNCs, all of which were sealed at 23 °C after cast. At the age of 28 days they were demolded and cut with a low-speed oil saw to expose a fresh surface. A lapping procedure at 45, 30, 15 μm with paraffin oil for 12 min each and a polishing procedure using 9, 6, 3, 1, 0.25 μm diamond paste for 20 min each on top of Texmet paper were conducted on the sample surface. These procedures are similar with the methods described elsewhere [13,14]. The nanoindentation tests were performed on the three different phases: the unhydrated cement particles, the high density CSH and the low density CSH with a TI 950 TriboIndenter [15] from Hysitron Corporation. For each test, multiple indents (greater than 5) were measured for each phase, and post indentation evaluation confirmed the location of each indent was in the desired phase. Fig. 2 shows a scanning probe microscopic (SPM) image obtained with the indenter at the scanning mode on a 50 μm × 50 μm sample surface: Fig. 2 (a) is the topographic image and (b) the gradient image. The triangular shaped particle in the middle of the figures is the unhydrated cement particle and the features in the relatively uneven area surrounding the particle are the hydration products. The dots with numbers show the locations where indentation was performed. In this case, locations 1–9 correspond to interfacial region, 10–15 to the unhydrated cement particle and 16–18 to the matrix (low density CSH). The distance between nanoindentations was maintained to be greater than ~10 μm in all these cases.

For all nanoindentation experiments, a single load function was applied with 4000 μN in load-controlled mode. The loading rate is 800 μN/s. Subsequently the load is kept constant for 5 s in order to minimize creep behavior within various phases of the paste matrix. Otherwise, the viscoelastic and creep properties can result in significant bowing in the unloading curves, which might affect the data analysis of nanoindentation. Unloading rate is 800 μN/s. In this given indentation experiment, the peak load (P_{max}), the contact depth at the peak load (h), and the slope of the unloading curve ($S = dP/dh$) were obtained. The reduced indentation modulus E_r was determined following [16]:

$$E_r = \frac{dP}{dh}\frac{\sqrt{\pi}}{2\sqrt{A}} \quad (1)$$

where A is the projected contact area, which needs to be calculated from the indenter geometry (Berkovich) and contact depth (h) based on previous calibration on the reference materials. dP/dh is the slope of unloading curve in the load-depth curve.

2.6. Scanning electron microscopy (SEM) and energy-dispersive X-ray (EDX) spectroscopy

The EDX technique has been widely employed for the elemental analysis on the chemical compositions of cement composites

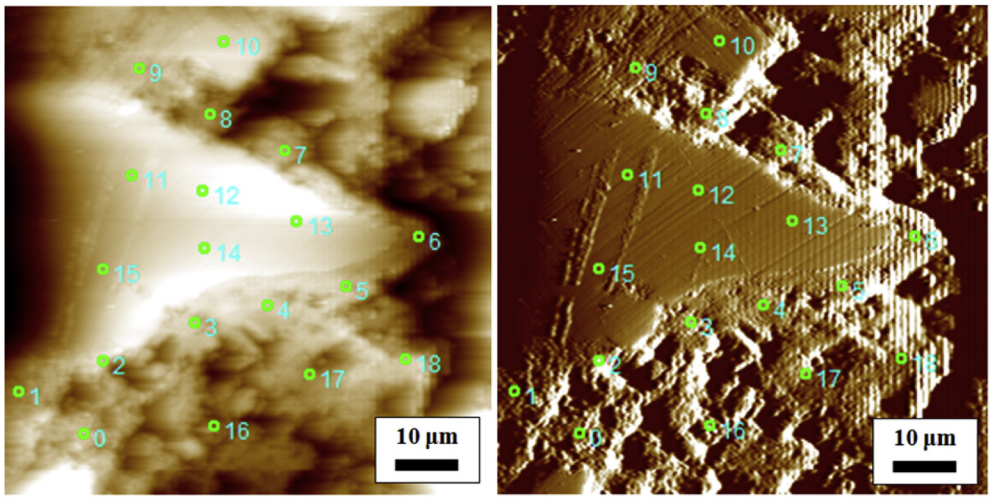

Fig. 2. The locations picked for the nanoindentation on the (a) topographic image; (b) gradient image on a 50 μm × 50 μm area.

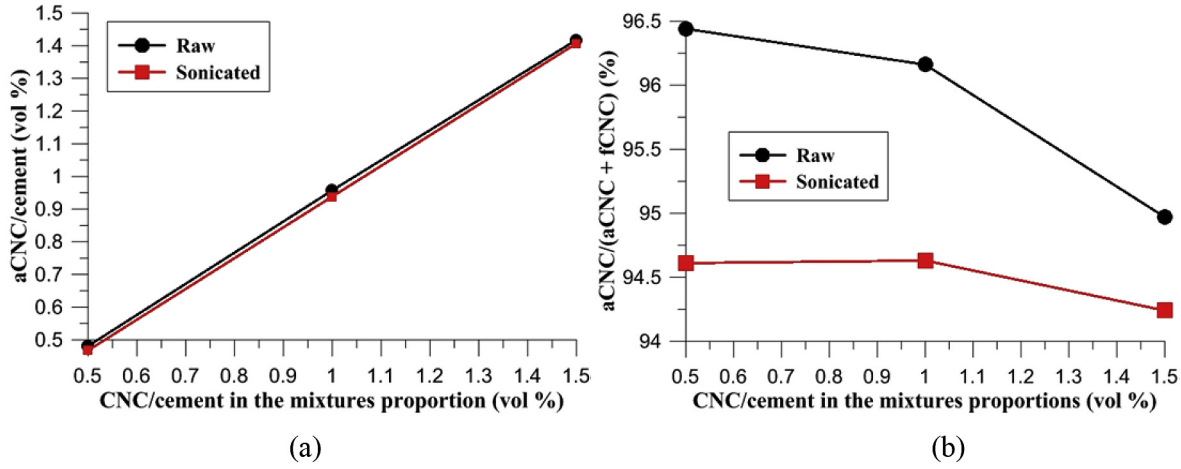

Fig. 3. (a) The mass of the aCNCs per gram of cement and (b) the aCNC percentages out of all CNCs.

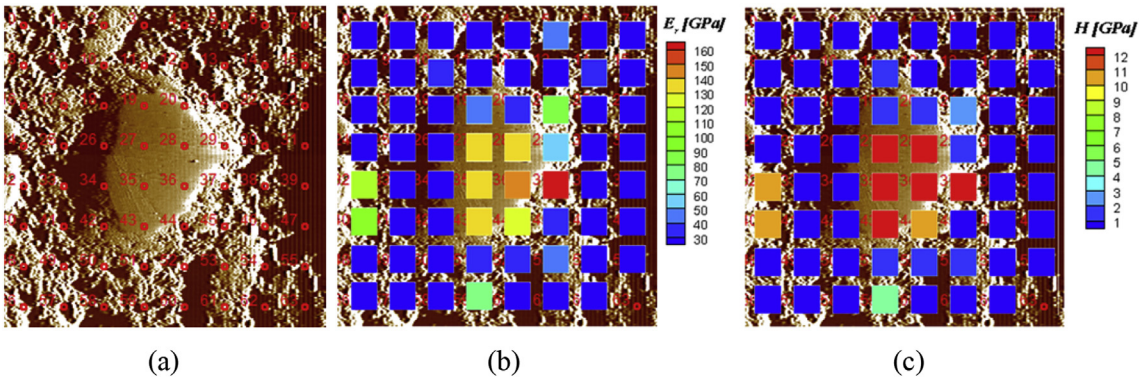

Fig. 4. (a) An area containing an unhydrated cement particle and matrix for the plain cement paste; the mapping of (b) reduced modulus and (c) hardness on this area.

[17–19]. In this work EDX was performed to investigate the CNC distribution in the hardened cement pastes with an FEI Quanta 3D FEG equipment. Three specimens were studied: the plain cement paste (reference), one with 1.5 vol % raw CNCs and one with 1.5 vol % sonicated CNCs. Ideally the element carbon should help to locate the CNCs in the cement pastes since cement does not contain carbon while CNCs ($(C_6H_{10}O_5)_n$) do. However, based on the preliminary EDX results, carbon was detected over the entire surface of the cement paste specimen, which was likely due to the carbonation [20,21], even when all the specimens were carefully stored in a desiccator. For this reason this work focuses on the oxygen spectroscopy and studies how the oxygen concentration fluctuates at different phases in the cement paste. As the condition for the imaging and EDX signal acquisition might be different for different specimens, the signal intensities cannot be directly compared with each other, and therefore a normalization was performed for the oxygen spectroscopy with the signals collected from the unhydrated cement cores as a base. Since the CNCs cannot penetrate into those cores, the chemical compositions as well as the oxygen concentration should be always the same at the core. With a normalization based on the oxygen concentration within the cores, the signals can be compared between EDX results for different specimens without taking into account of the experimental conditions. The normalization of the signal counts was done with following procedures: The oxygen signals collected within the unhydrated cement cores were picked and the average count (intensity) in this region was calculated as N_{ave}, and then all the original oxygen signal intensity I_{ori} in the same mapping were divided by N_{ave} to obtain the normalized intensity I_{nor}, as shown in following equation:

$$I_{nor} = \frac{I_{ori}}{N_{ave}} \tag{2}$$

2.7. Water desorption

The equilibrium relative humidity (RH_{eq}) at which the transition happens between condensation and evaporation of the liquid inside a pore can be related with the pore radius and the liquid properties with the well-known Kelvin equation [22,23]:

$$\ln(RH_{eq}(r)) = \frac{rRT}{2\gamma V_m} \tag{3}$$

where γ is the surface tension, V_m the molar volume of the fluid, R the universal gas constant, r the radius of the pore, T the temperature. The water desorption with a decreasing RH for the water saturated hardened cement paste was measured with a Q5000 SA absorption/desorption analyzer from TA instruments. Three different specimens were studied: plain cement paste, a cement paste with 1.5 vol % raw CNCs and a cement paste with 1.5 vol % sonicated CNCs. The cement pastes were demolded at the age of 28 days and a 1-mm thick specimen was obtained with a low-speed oil

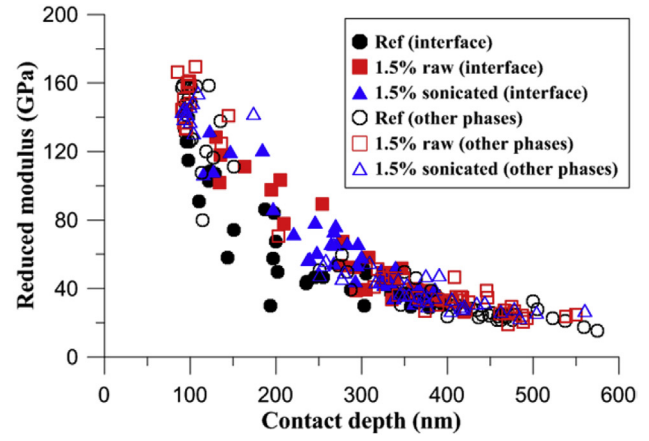

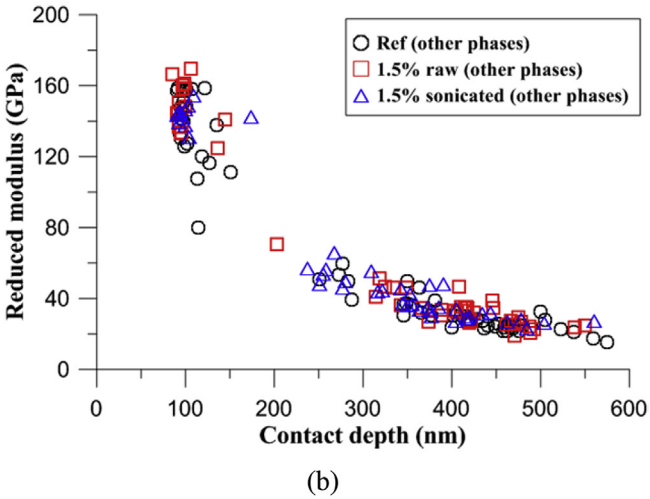

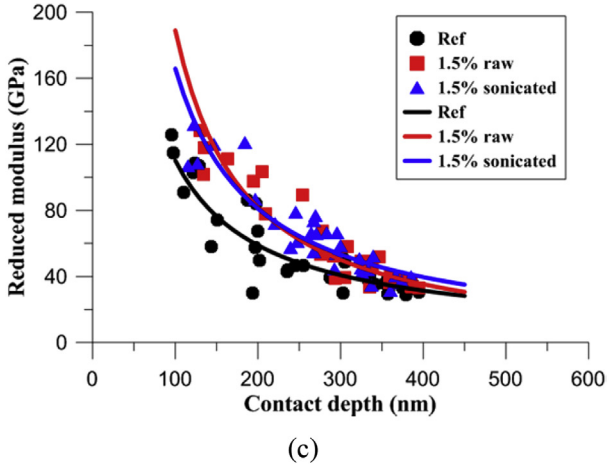

Fig. 5. The relationship between the reduced modulus and contact depth (a) at all three different phases; (b) at the unhydrated cement and low density CSH; (c) at the interfacial regions.

saw. The specimens were vacuum saturated by placing them in a desiccator and evacuating the air for 8 h, and then back-filled with vacuum de-gassed for another 3 h. After taken out from the vacuumed water, the surface moisture of the fully saturated specimens were wiped with a Kimwipes delicate task wiper mildly and quickly (within ~3 s) and then the specimens were immediately transferred

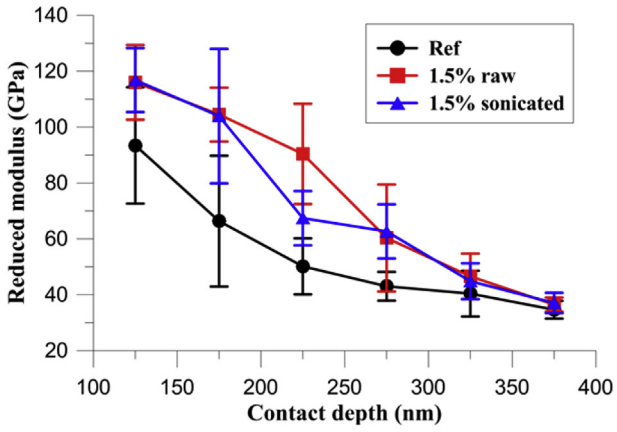

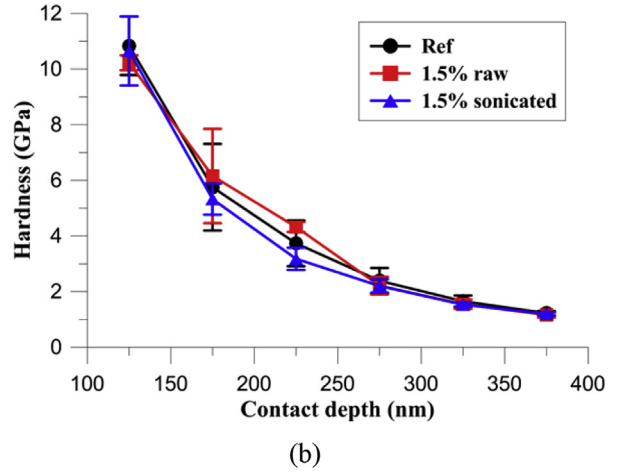

Fig. 6. (a) The average reduced modulus and (b) the average hardness on the interfacial regions.

to the equipment to avoid the evaporation of the water from pores. The initial RH in the chamber was 97.5%, and then the RH was decreased with 10% steps, and a final step of 17.5% to reach 0%.

3. Results and discussions

3.1. The concentration of aCNCs and fCNCs

The amount of aCNCs and fCNCs adhered on the cement particles was quantified by the centrifugation method described in Section 2.3. We analyzed three different concentrations: 0.5 vol %, 1.0 vol % and 1.5 vol % with and without sonication (raw) (Mixtures #5, 6 and 7 in Table 2). Fig. 3 (a) shows the mass of the aCNCs per gram of cement and (b) gives the aCNC percentages out of all CNCs, i.e., aCNCs/(fCNC + aCNCs) %. The results in Fig. 3 (a) indicate that, with increasing the CNC concentration (from 0.5 vol % to 1.5 vol %) the aCNC/cement percentage increases almost linearly and is not affected by sonication. This means that the CNCs keep adsorbing on the cement surface. Fig. 3 (b) shows that the percentage of the aCNCs out of all CNCs does not change much, and is not necessarily affected by sonication (within measurement uncertainty). In conclusion, the majority of the CNCs (94.2%–96.5%) are adsorbed on the cement surface, regardless of the total amount of CNCs added in the cement paste. This result suggests that, while sonication disperses CNC agglomerates [4], it does not exchange aCNCs for fCNCs.

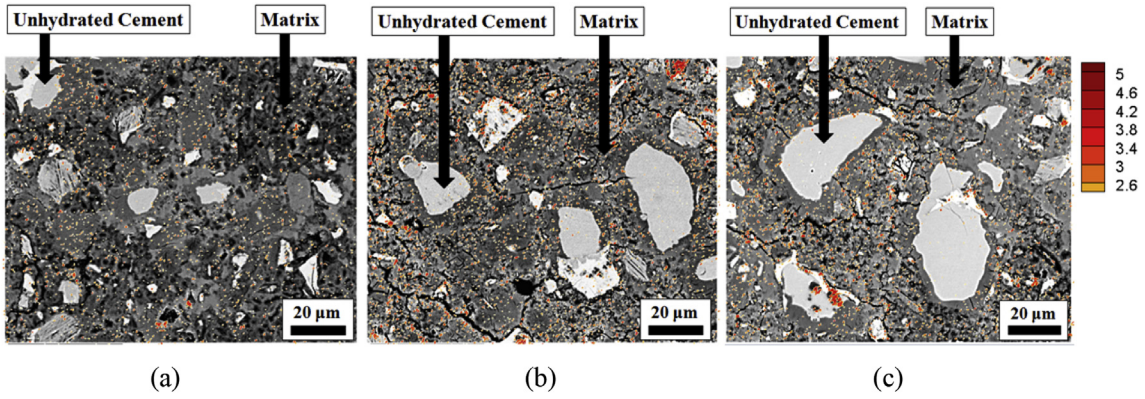

Fig. 7. Oxygen mapping with SEM images of (a) plain cement paste; (b) with 1.5 vol % raw CNCs and (c) with 1.5 vol % sonicated CNCs.

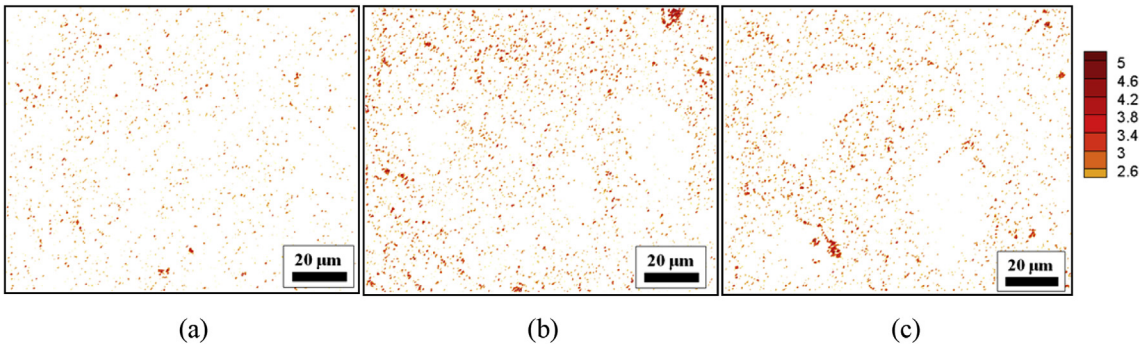

Fig. 8. Oxygen mapping alone of (a) plain cement paste; (b) with 1.5 vol % raw CNCs and (c) with 1.5 vol % sonicated CNCs.

A simple calculation is given here to estimate the maximum surface area of cement particles that can be covered by CNCs with an assumption that all the CNCs lie on the surface with one of their sides and there is no overlapping of CNCs. Assume the total mass of all CNCs is m, and the total volume as m/density, then the total length of all CNCs is $L = (m/\text{density})/(\text{CNC cross-section})$. Given that the cross-section of the CNC is approximately 4×4 nm^2 square (the width can range from 3 to 5 nm according to [1]), the maximum area covered with CNCs is then $A = L \times 4$ nm. For every kg of cement, at the CNC/cement vol concentrations of 0.5%, 1.0% and 1.5%, the maximum surface coverage by CNCs (m^2/kg) is calculated as 400, 800, and 1200 m^2, respectively. As the Blaine fineness (surface area per unit kg cement) of the cement used in this work is 316 m^2/kg, CNCs can cover all the surface of cement for the three concentrations in this ideal situation. However, this calculation does not account for the fCNCs, and more important, the overlapping of the aCNCs on the cement surface, which is highly possible given the agglomeration of CNCs in the fresh cement paste [2]. For these reasons, the actual area covered by CNCs should be smaller than the values calculated above, and is also smaller than the total surface area of cement, given that the adsorption continues to occur without reaching any limit (Fig. 3 (a)).

3.2. Nanoindentation

Nanoindentation was performed to study the CNCs distribution in the cement pastes at an age of 28 days and their influence on the local mechanical properties. Three different specimens were analyzed: the plain cement paste, one with 1.5 vol % raw CNCs and one with 1.5 vol % sonicated CNCs. A representative mapping of the reduced modulus and hardness is shown in Fig. 4. As expected, the unhydrated cement particle shows much higher reduced modulus and hardness than the matrix phase [24].

As stated earlier, the interfacial region between the unhydrated cement and the matrix is likely to contain the highest concentration of CNCs, and therefore is the phase of main interest. The reduced modulus is plotted as a function of the contact depth as shown in Fig. 5(a) for all the three different phases, from which it can be observed that for the three different specimens, the reduced moduli are close at the cement particle and matrix phase. This can be more clearly observed in Fig. 5(b), which shows the data obtained only from the low density CSH and the unhydrated cement. Finally, Fig. 5(c) shows the reduced modulus for the interfacial regions. In the plots the data on the interfacial region are designated as the solid symbols and the data from the other two phases (unhydrated cement and matrix) are open symbols. The data in Fig. 5(c) are fit with a power law and the two specimens with CNCs show trendlines which are higher than the reference. The fitting equations are given as:

$$\text{Ref}: \quad y = 7119x^{-0.91} \tag{4}$$

$$1.5\%\ \text{raw}: \quad y = 49714x^{-1.21} \tag{5}$$

$$1.5\%\ \text{sonicated}: \quad y = 19309x^{-1.03} \tag{6}$$

The reduced modulus results indicate that the unhydrated cement and low density CSH are not affected much by CNCs, which is expected since most CNCs are in the high density CSH. Moreover on the high density CSH, the reduced modulus is improved with raw and sonicated CNCs.

The reduced modulus and the hardness for the interfacial regions are grouped based on the contact depth with a bin size of 50 nm to obtain average values. For example, the reduced moduli

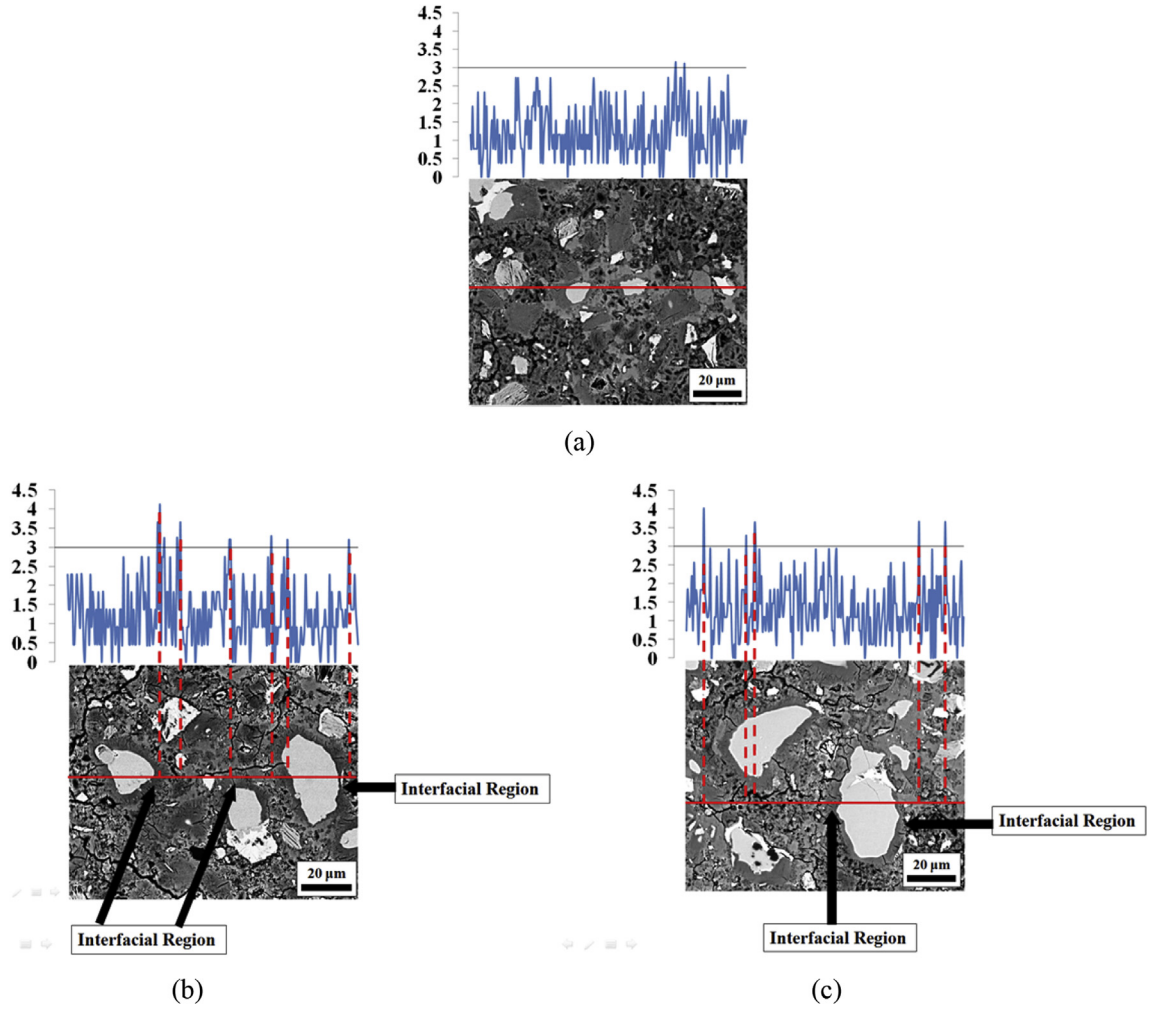

Fig. 9. Line-scanning spectroscopy of oxygen of (a) plain cement paste; (b) with 1.5 vol % raw CNCs and (c) with 1.5 vol % sonicated CNCs.

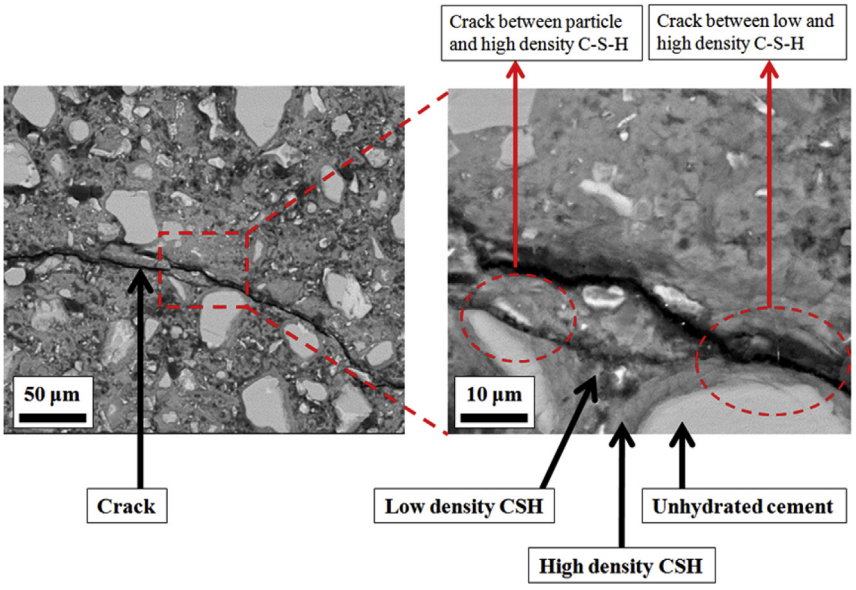

Fig. 10. SEM images show multiple cracks in the cement paste with 1.5 vol % raw CNCs.

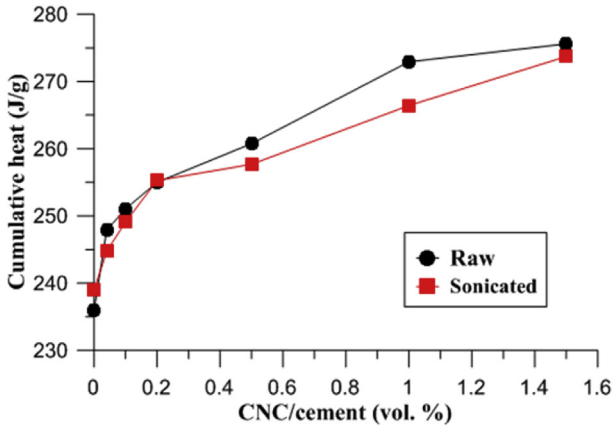

Fig. 11. Cumulative heats comparison between the cement pastes with raw and sonicated CNCs at the age of 168 h.

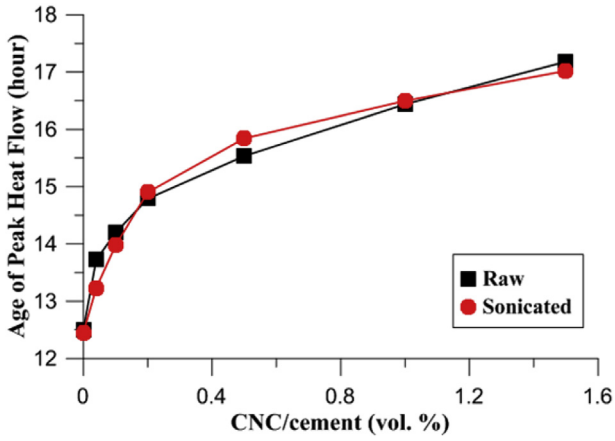

Fig. 12. The ages of the peak flow of the cement pastes with raw and sonicated CNCs.

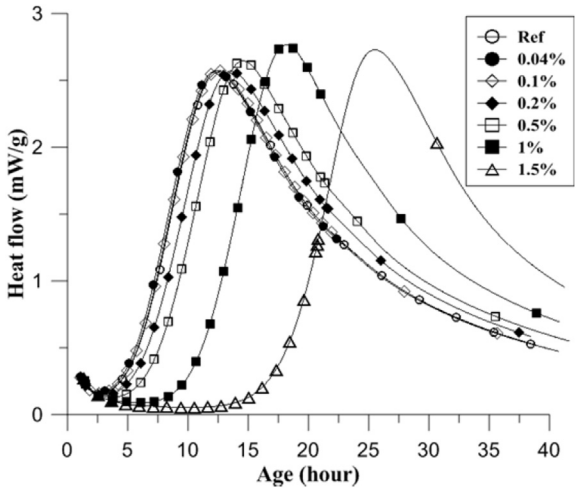

Fig. 13. Heat flow curves of cement pastes with WRA.

within the contact depth between 100 and 150 nm are grouped to calculate the average reduced modulus, which is then reported by the average contact depth 125 nm in Fig. 6. Fig. 6 (a) shows that with CNC additions, the reduced modulus is increased significantly compared with the plain cement paste (reference), especially below the contact depth of 300 nm. For example, the average reduced modulus for the contact depth 150–200 nm was increased from ~70 GPa to ~105 GPa with CNC additions, which is 50% improvement. The reason for the improvements may be the high elastic modulus of CNCs, which ranges from 110 to 220 GPa [1,25,26], which is higher than that of the interfacial region (high density CSH) with the value about 40–110 GPa. If it is assumed that the mechanical properties of the "composites" constituted by the high density CSH and the CNCs follow a mixtures law, the modulus of high density CSH can be increased by CNCs. Another possible reason is that CNC additions caused a modification to the CSH (e.g. its structure, or chemistry, etc.) which may also have altered the modulus. Fig. 6 (b) shows that with CNC additions, the hardness does not change much in the interfacial regions, the maximum change with respect to the reference is ~10%, which is much smaller than the influence in the reduced modulus.

3.3. EDX and SEM

The results of the oxygen mapping for the three specimens are shown in Fig. 7 overlapping the original SEM images and the mappings without SEM images are provided in Fig. 8. In the mapping, the signals with intensity below 2.6 (this chosen value is approximately the smallest number that the oxygen signals inside the unhydrated cement can be removed) are truncated and only the signals above that are shown (higher intensity means higher oxygen concentration). From Fig. 8 (a) it can be observed that only very few oxygen signals are observed inside the unhydrated cement cores compared with the matrix phase. This difference is due to the oxygen from chemically bound water in the hydration products. By comparing the mappings between the reference and the two specimens with CNCs (Fig. 8b and c), it is found that the oxygen concentration is much higher in the matrix phase and the interfacial region, which indicates the distribution of CNCs. Based on the visualization, however, it is difficult to observe a significant difference between the specimens with raw and sonicated CNCs. Oxygen spectroscopy is performed along a scanning-line (red) across one or more unhydrated cement particles to make a quantitative comparison between the three specimens, as shown in Fig. 9. For the plain cement paste (reference), the spectroscopy is relatively stable that most of the peaks are below the intensity of 3, while the two specimens with CNCs, there are a few high peaks which are highlighted with dashed lines denoting their corresponding locations in the cement pastes (the intensity of 3 is plotted with the thin black line in Fig. 9). It is noteworthy that the locations of the peaks are different for the specimens with raw and sonicated CNCs. For the one with raw CNCs, most of the peaks are found at the interfacial region between cement particle and the matrix, while for the one with sonicated CNCs, the peaks are randomly distributed along the scanning line. This result indicates that, without sonication, a high concentration of CNCs (aCNCs) are prone to stay at the interfacial region, while after sonication they are more randomly dispersed into the matrix phase.

As previously discussed, most of the CNCs are adsorbed on the cement surface in the fresh cement paste regardless of whether sonication was employed. However the CNCs cannot be distinctly classified as the aCNCs or fCNCs in the hardened cement paste. In fact, CNCs are found distributed in the matrix phase, both high and low density CSH. This fact means that, during the CSH growth, some of the aCNCs are embedded in the high density CSH while some others move away from the cement particles into the low density region (matrix phase), which is similar with the case of fCNCs.

Multiple cracks are observed from the SEM images. Fig. 10 shows an example of the cement paste with raw CNCs. It can be observed that, the cracks pass through two different paths: one between the unhydrated cement particle and the high density CSH, and the

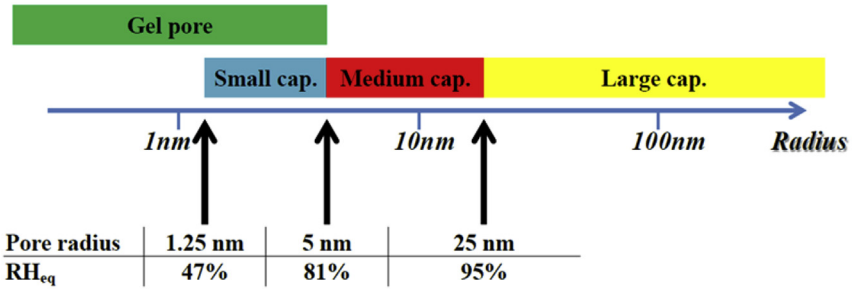

Fig. 14. The size ranges of different pores and the corresponding RH_{eq}.

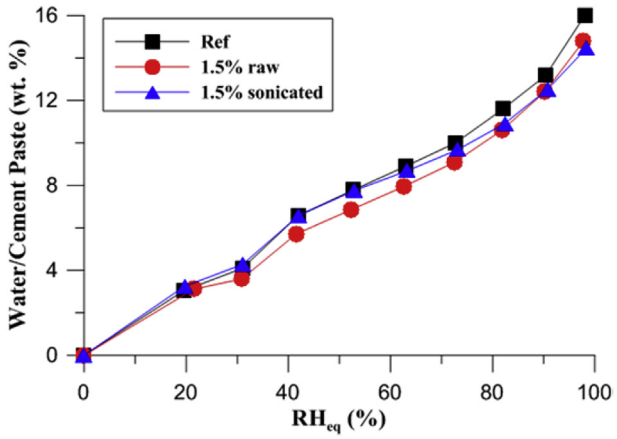

Fig. 15. The relationship between the water content and the RH_{eq}.

other between low (matrix phase) and high density CSH, as circled in Fig. 10. The SEM images here may indicate that the crack can randomly pass through different interfaces regardless of CNC concentrations.

3.4. Isothermal calorimetry

The cumulative heat release at the age of 168 h are summarized in Fig. 11 and the values are generally very similar for different concentrations. Fig. 12 summarizes the relationship between the ages of the heat flow peak with the CNC concentration for the two different CNCs, which shows that the delay in hydration is not influenced much by sonication. As a summary, the cement pastes with raw and sonicated CNCs do not show significant differences in the cumulative heats at the age of 7 days (168 h) or the hydration processes. This seems to indicate that although the CNCs are more dispersed with sonication, the effect of SCD as a whole is not affected significantly. This result is not unexpected since it was found that after sonication, the concentration of aCNCs did not appear to change much.

In the previous paper [2], it was established that steric stabilization is one of the mechanisms that CNCs use to improve the DOH, which is similar with what the polycarboxylate-based water-reducing agent (WRA) does in the cement paste. A parallel hydration study was performed on the cement pastes with varying dosages of a polycarboxylate-based WRA (ADVA 140). As expected, with WRA, the dormant period is significantly extended as shown in Fig. 13 that, the heat flow peak delay for the 1.5 vol % WRA cement paste is about 15 h, which is much longer than that of the 1.5 vol % CNC cement paste (~4.5 h). This is because the hydrophobic chains [27] of the WRA block water from reaching the cement surface, while the hydrophilic and hygroscopic nature of CNCs [3] lead to SCD, although both WRA and CNCs can be adsorbed on the cement surface.

3.5. Pore size distribution

Water desorption tests were performed to study the CNCs influence on the pore size distribution of the cement pastes. Mindness et al. [28] classified pores with respect to the pore radius: small capillary pores (cap.) of 1.25 nm–5 nm, medium capillary pores 5–25 nm, large capillary pores >25 nm and gel pores with the radius below 5 nm. In the work by Villani et al. [22], they provided a plot of the relationship between the pore radius and the RH_{eq} of water based on the Kelvin Equation. Fig. 14 summarizes the pore size ranges of different types of pores and the RH_{eq} values corresponding to the boundaries of different pores.

The water content as a function of RH_{eq} is shown in Fig. 15 for the three specimens. The two specimens with CNCs show a reduction in the water content compared with the plain cement paste. This result is expected, as CNCs can improve the DOH of

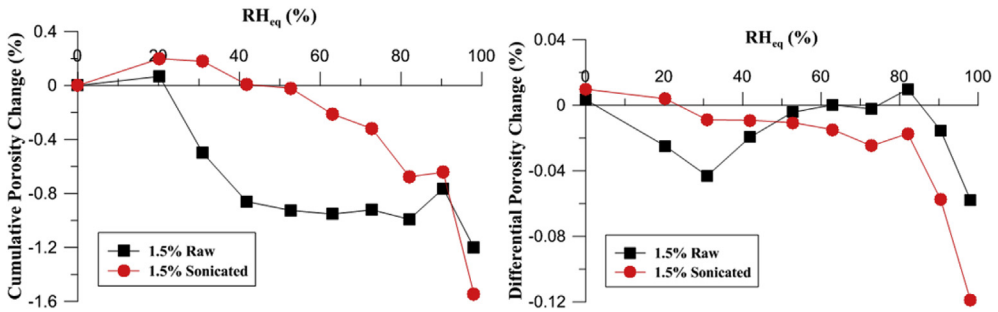

(a) (b)

Fig. 16. (a) The cumulative porosity change and (b) the differential porosity change of the cement pastes with raw and sonicated CNCs from the reference.

cement paste, and a consequent result is the reduction of the total porosity.

The porosity differences (in percentage) between the specimens with CNCs and plain cement paste (reference) at different RH_{eq} are plotted versus the RH_{eq} in both cumulative and differential values are shown in Fig. 16. The total porosity reductions (at the $RH_{eq} = 97.5\%$) for the cement pastes with raw and sonicated CNCs are 1.2% and 1.6%, respectively. Without sonication, the CNC agglomerates adsorb water and the unreacted water may form the capillary pores. In addition, the CNC agglomerates may bring air entrapment which also increases porosity. As a result, the porosity reduction with sonicated CNCs is larger than that with raw CNCs. For high values of RH_{eq} (>50%), the sonicated CNCs reduce the porosity when compared to the raw ones because there are fewer CNC agglomerates and the dispersed single CNCs cannot cause either high concentration of water around them or air entrapment. However, at the low RH_{eq} region (<50%), the raw CNCs lead to more pore reduction than the sonicated CNCs. Within this RH_{eq} range, the pores are classified as the small gel pores (Fig. 14), which are included in the space occupied by the hydration products [28]. The results in Fig. 16 may indicate that the dispersed single CNCs lead to a certain amount of gel pores around them. In summary, CNC agglomerates attract a large amount of water, which lead to capillary pores, while single CNCs attract a small amount of water, which lead to gel pores.

3.6. Discussion

The centrifugation experiment indicates that after sonication, the majority of the CNCs are still the aCNCs. It is observed from the calorimetry results that the hydration process is not influenced much with sonication, which is consistent with the centrifugation result. Given that the CNC agglomerates are reduced with sonication, it appears that the aCNCs are more uniformly distributed on cement surface after sonication. EDX results verifies this hypothesis that for raw CNCs, the oxygen is more concentrated on the high density CSH, while with sonication, CNCs are more dispersed. The pore size distribution study shows that sonication helps reduce the porosity at the large size range, i.e., the capillary pores, which is also a result of the reduction in agglomerates. The nanoindentation results also indicate that there are high concentrations of CNCs in the high density CSH and the reduced modulus at the high density CSH is increased with CNC additions.

4. Conclusions

This paper studies how sonication influences the CNCs distribution in both fresh and hardened cement pastes and how it modifies the microstructures of the pastes. Although sonication can disperse the CNC agglomerates, the dispersed CNCs remain adsorbed on cement surface in the fresh cement paste. For the hardened cement paste, it is found that sonication helps reduce the large size porosity. The nanoindentation results show that the reduced modulus at the high density CSH is increased with CNC additions, possibly due to the high modulus of the CNCs.

Acknowledgements

This work was supported by the National Science Foundation through Awards no. CMMI #1131596. The authors are grateful for the USFS Forest Products Laboratory for providing the CNC materials.

References

[1] R.J. Moon, A. Martini, J. Nairn, J. Simonsen, J. Youngblood, Cellulose nanomaterials review: structure, properties and nanocomposites, Chem. Soc. Rev. 40 (7) (2011) 3941–3994.
[2] Y. Cao, P.D. Zavattieri, J. Youngblood, R.J. Moon, J. Weiss, The influence of cellulose nanocrystal additions on the performance of cement paste, Cem. Concr. Compos 56 (2015) 73–83.
[3] R.M. Taib, Cellulose Fiber-reinforced Thermoplastic Composites: Processing and Product Characteristics, Virginia Polytechnic Institute and State University, Blacksburg, Virginia, 1998.
[4] Y. Cao, P.D. Zavattieri, J. Youngblood, R.J. Moon, J. Weiss, The relationship between the dispersion of cellulose nanocrystals and strength improvements. In Preparation for Construction and Building Materials.
[5] F.P. Laboratory, Nanocellulose Pilot Plant, Forest Products Laboratory, 2009. http://www.fpl.fs.fed.us/.
[6] X.M. Dong, J.-F. Revol, D.G. Gray, Effect of microcrystallite preparation conditions on the formation of colloid crystals of cellulose, Cellulose 5 (1) (1998) 14.
[7] D. Bondeson, A. Mathew, K. Oksman, Optimization of the isolation of nanocrystals from microcrystalline cellulose by acid hydrolysis, Cellulose 13 (2) (2006) 10.
[8] F. Rajabipour, G. Sant, J. Weiss, Interactions between shrinkage reducing admixtures (SRA) and cement paste's pore solution, Cem. Concr. Res. 38 (5) (2008) 606–615.
[9] TA-Instruments, TAM Air Isothermal Calorimetry, TA-Instruments, 2013. http://www.tainstruments.com/main.aspx?siteid=11&id=217&n=4.
[10] W. Li, J. Xiao, Z. Sun, S. Kawashima, S. Shah, Interfacial transition zones in recycled aggregate concrete with different mixing approaches, Constr. Build. Mater 35 (2012) 1045–1055.
[11] P. Acker, Micromechanical analysis of creep and shrinkage mechanisms, in: F. Ulm, Z. Bažant, F. Wittman (Eds.), Creep, Shrinkage and Durability Mechanics of Concrete and Other Quasi-brittle Materials, Elsevier, Oxford, UK, 2001.
[12] L. Sorelli, G. Constantinides, F. Ulm, F. Toutlemonde, The nano-mechanical signature of ultra high performance concrete by statistical nanoindentation techniques, Cem. Concr. Res. 38 (12) (2008) 1447–1456.
[13] W. Ashraf, J. Olek, N. Tian, Nanomechanical characterization of the carbonated wollastonite system, in: Fifth International Symposium on Nanotechnology in Construction, 2015, p. 7.
[14] J.J. Hughes, P. Trtik, Micro-mechanical properties of cement paste measured by depth-sensing nanoindentation: a preliminary correlation of physical properties with phase type, Mater Charact. 53 (2–4) (2004) 9.
[15] Hysitron. http://www.hysitron.com/products/ti-series/ti-950-triboindenter.
[16] W. Oliver, G. Pharr, An improved technique for determining hardness and elastic modulus using load and displacement sensing indentation experiments, J. Mater Res. 7 (6) (1992) 20.
[17] C. Famy, A. Brough, H. Taylor, The C-S-H gel of portland cement mortars: part I. the interpretation of energy-dispersive X-ray microanalyses from scanning electron microscopy, with some observations on C-S-H, AFm and AFt phase compositions, Cem. Concr. Res. 33 (2003) 1389–1398.
[18] S. Diamond, Identification of hydrated cement constituents using a scanning electron microscope - energy dispersive X-ray spectrometer combination, Cem. Concr. Res. 2 (1972) 16.
[19] H.G. McWhinney, D.L. Cocke, K. Balke, J.D. Ortego, An investigation of mercury solidification and stabilization in portland cement using X-ray photoelectron spectroscopy and energy dispersive spectroscopy, Cem. Concr. Res. 20 (1990) 3.
[20] F.-A. Sarott, M.H. Bradbury, P. Pandolfo, P. Spieler, Diffusion and adsorption studies on hardened cement paste and the effect of carbonation on diffusion rates, Cem. Concr. Res. 22 (2–3) (1992) 439–444.
[21] S.E. Pihlajavaara, E. Pihlman, Effect of carbonation on microstructural properties of cement stone, Cem. Concr. Res. 4 (2) (1974) 149–154.
[22] C. Villani, R. Spragg, M. Pour-Ghaz, W.J. Weiss, The influence of pore solutions properties on drying in cementitious materials, J. Am. Ceram. Soc. 97 (2) (2014) 386–393.
[23] J. Castro, P. Lura, F. Rajabipour, R. Henkensiefken, J. Weiss, Internal curing: discussion of the role of pore solution on relative humidity measurements and desorption of lightweight aggregate (LWA), ACI Spec. Publ. 270 (2010) 89–100.
[24] G. Constantinides, F.-J. Ulm, The effect of two types of C-S-H on the elasticity of cement-based materials: results from nanoindentation and micromechanical modeling, Cem. Concr. Res. 34 (2004) 14.
[25] F. Dri Jr., L.G. Hector, R.J. Moon, P.D. Zavattieri, Anisotropy of the elastic properties of crystalline cellulose Iβ from first principles density functional theory with van der Waals interactions, Cellulose 20 (6) (2013) 16.
[26] F.L. Dri, S. Shang Jr., L.G. Hector, P. Saxe, Z.-K. Liu, R.J. Moon, et al., Anisotropy and temperature dependence of structural, thermodynamic, and elastic properties of crystalline cellulose Iβ: a first-principles investigation, Modell. Simul. Mater Sci. Eng. 22 (8) (2014) 1–28.
[27] M. Medeiros, P. Helene, Efficacy of surface hydrophobic agents in reducing water and chloride ion penetration in concrete, Mater Struct. 41 (2008) 13.
[28] S. Mindess, J.F. Young, D. Darwin, Concrete, Pearson Education, Inc, 2002.